DETECTING THE AFFECTED AREAS OF MOUNT SINABUNG ERUPTION USING LANDSAT 8 IMAGERIES BASED ON REFLECTANCE CHANGE

Suwarsono, Hidayat, Jalu Tejo Nugroho, Wiweka, Parwati, and M. Rokhis Khomarudin
Remote Sensing Applications Center,
Indonesian National Institute of Aeronautics and Space (LAPAN)
e-mail: suwarsono@lapan.go.id/landsono@yahoo.com
Received: 26 February 2015; Revised: 7 April 2015; Approved: 11 May 2015

Abstract. The position of Indonesia as part of a "ring of fire" bringing the consequence that the life of the nation and the state will also be influenced by volcanism. Therefore, it is necessary to map rapidly the affected areas of a volcano eruption. Objective of the research is to detect the affected areas of Mount Sinabung eruption recently in North Sumatera by using optical images Landsat 8 Operational Land Imager (OLI). A pair of Landsat 8 images in 2013 and 2014, period before and after eruption, was used to analysis the reflectance change from that period. Affected areas of eruption was separated based on threshold value of reflectance change. The research showed that the affected areas of Mount Sinabung eruption can be detected and separated by using Landsat 8 OLI images based on the change of reflectance value band 4, 5 and NDVI. Band 5 showed the highest values of decreasing and band 4 showed the highest values of increasing. Compared with another uses of single band, the combination of both bands (NDVI) give the best result for detecting the affected areas of volcanic eruption.

Keywords: *affected area, Landsat 8, NDVI, Mount Sinabung, reflectance*

1 INTRODUCTION

Mount Sinabung is an active stratovolcano, located in Karo Regency, North Sumatra Province (Figure 1-1). This volcano is classified as B-Type volcano because there was no eruptive activity since 1600's (Kusumadinata, 1979). Since its latest eruption about 1,200 year ago, a phreatic eruption occurred on August 27, 2010. The eruption was initiated by a greyish white plume and then followed by black plumes as high as 2000 m above the crater. Altered rock fragments and ash were erupted during this event. With regard to these activities, the Head of Centre for Volcanology and Geological Hazard Mitigation classifies Mount Sinabung into A-Type volcano (Sutawidjaja *et al.*, 2013).

According to the records of the Center for Volcanology and Geological Hazard Mitigation, in the middle-end of 2013, this volcano erupted again. On November 3, 2013, raised the level of alert activity into '*Siaga*' (Stand-by). Then raised again to '*Awas*' (Caution - the highest alert for volcanic activity) on November 24, 2013 at 10:00 am due to the significantly increased volcanic activity. The recent volcanism activity was commenced on 8 April 2014 at 5:00 PM, when Mount Sinabung level of activity decreased from level of '*Awas*' into '*Siaga*'.

According to the Center for Volcanology and Geological Hazard Mitigation, the potential hazard of the eruption of Mount Sinabung up to 11 September 2014 can be derived from lava flows, incandescent lava and hot clouds that leads to the south and southeast as far as 5 kilometers. In addition, there is the potential for secondary hazards from lahar that may occur due to high rainfall that is capable of transporting ash fall, tephra, lava debris, rock fragments through the river valleys. Attention to the potential hazard of this, it is important to know the distribution of eruptive material and the damage that has been caused.

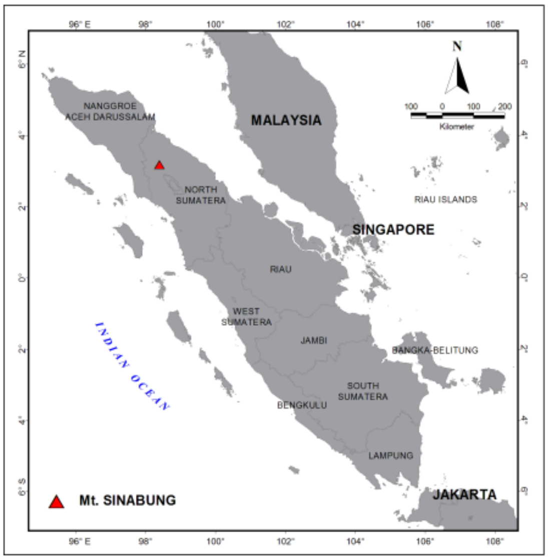

Figure 1-1: Location of the Mt. Sinabung in North Sumatera Province.

The Landsat series of satellites has provided the long continuous data of the volcanoes activities in the world since 1972. The calculation of total thermal flux for lava flowing in tubes, on the surface, or under shallow water has been done by using Landsat TM (Harris et al., 1998). The Landsat ETM$^+$ data can be use for understand the thermal characteristics of a series of lava flows emplaced at Mount Etna volcano, Sicily, during 27–28 October 1999, by examining the composition of the short-wave infrared (SWIR) signal emitted from the flow surface (Wright et al., 2001). The TM data also was used to delineate the geomorphic features of the island of Lesvos, Greece (Novak et al., 2000). The Landsat ETM$^+$ also can be use to recognize the morphological changes in the drainage system and lahar detection. For lahar delineation, the principal components analysis and canonical classification (Tasseled Cap) in order to perform a supervised image classification using the maximum likelihood rule algorithm can be use to delienate the lahar (Davila et al., 2007). With higher spatial resolution panchromatic data, the Landsat 7 ETM$^+$ able to map lava flow fields, trace very high temperature lava channels, and identify an arcuate feature associated with a collapsed crater floor, a phenomenon that may precede explosive activity. With improved spatial resolution in the thermal IR, the data also able to map the bifurcation and braiding of underground lava tubes and estimate effusion rates (Flynn et al., 2001). Landsat 7 ETM$^+$ also was used to map the the Nyamulagira lava flows from 1938 up to the last eruption to date in 2010 (Benoît et al., 2010). The fractional area of the hottest part of an active flow and the temperature of the cooler crust of Mount Etna eruptions were estimated using for two shortwave infrared Landsat Thematic Mapper (TM) (Lombardo et al., 2004). This research aims to detect the affected areas of Mount Sinabung eruption recently in North Sumatera by using optical images Landsat 8 Operational Land Imager.

Landsat 8 satellite or LDCM (Landsat Data Continuity Mission) is the latest generation of Landsat satellite series. The satellite was developed by the National Aeronautics and Space Administration (NASA) and United States of Geological Survey (USGS) - Department of the Interior (DOI). The advantages of the satellites Landsat 8 compared to its predecessors is that it carries a charge sensor, which consists of sensor Operational Land Imager (OLI) and the Thermal Infrared Sensor (TIRS). OLI sensor consists of nine spectral channels with a spatial resolution of 30 m (15 m for the panchromatic channel) with a width of 185 km coverage (Table 1-1). The widths of several OLI bands are refined to avoid atmospheric absorption features within ETM$^+$ bands. The biggest change occurs in OLI band 5 (0.845–0.885 µm) to exclude a water vapor absorption feature at 0.825

μm in the middle of the ETM^+ near infrared band (band 4; 0.775–0.900 μm). The OLI panchromatic band, band 8, is also narrower relative to the ETM^+ panchromatic band to create greater contrast between vegetated areas and surfaces without vegetation in panchromatic images.

Additionally, two new bands are specified for the OLI; a blue band (band 1; 0.433–0.453 μm) principally for ocean color observations in coastal zones and a shortwave infrared band (band 9; 1.360–1.390 μm) that falls over a strong water vapor absorption feature and will allow the detection of cirrus clouds within OLI images (cirrus clouds will appear bright while most land surfaces will appear dark through cloud-free atmospheres containing water vapor) (Irons *et al.*, 2012).

The Thermal Infrared Sensor (TIRS) will measure land surface temperature in two thermal bands (Table 1-2). TIRS requirements are specified in a manner similar to the OLI requirements. The two bands were selected to represent an advancement over the single-band thermal data collected by previous Landsat satellites (the ETM^+ and TM sensors collect data for a 10.0–12.5 μm thermal band). The 120 m spatial resolution is a step back from the 60 m ETM^+ thermal band resolution and was specified as a compromise to the necessity of a rapid sensor development. The 120 m resolution is deemed sufficient for water consumption measurements over fields irrigated by center pivot systems. The instrument design exceeds requirements with a 100 m spatial resolution (Irons *et al.*, 2012).

Table 1-1: Comparison between OLI and ETM+ spectral band (Irons *et al.*, 2012)

OLI spectral bands			**ETM^+ spectral bands**		
Bands	Band with (μm)	GSD (m)	Bands	Band with (μm)	GSD (m)
1	0.433 – 0.453	30			30
2	0.450 – 0.515	30	1	0.450 – 0.515	30
3	0.525 – 0.600	30	2	0.525 – 0.605	30
4	0.630 – 0.680	30	3	0.630 – 0.690	30
5	0.845 – 0.885	30	4	0.775 – 0.900	30
6	1.560 – 1.660	30	5	1.550 – 1.750	30
7	2.100 – 2.300	30	7	2.090 – 2.350	30
8	0.500 – 0.680	15	8	0.520 – 0.900	15
9	1.360 – 1.390	30			

Table 1-2: TIRS spectral bands and spatial resolution (Irons *et al.*, 2012)

Bands	**Center wavelength (μm)**	**Minimum lower band edge (μm)**	**Maximum upper band edge (μm)**	**Spatial resolution (m)**
10	10.9	10.6	11.2	100
11	12.0	11.5	12.5	100

2 MATERIALS AND METHODOLOGY

2.1 Data

A pair of Landsat 8 OLI acquisition the Sinabung Volcano region used in this study, ie path/row 129/058. The first image dated June 7, 2013 and the second image dated March 22, 2014. The first image shows the condition before the eruption of November 2013 and the second image shows the condition after the eruption of that period. So, the detection focusses on the affected areas by eruption which were happened between 7th of June 2013 and 22th of March 2014 (Figure 2-1). We also use the Digital Elevation Model Shuttle Radar Topography Mission (DEM SRTM) 30 m resolution to understand the topography condition and to correct the reflectance due to topograhic effects.

2.2 Convertion Digital Number to Reflectance

The Landsat 8 consist of quantized and calibrated scaled Digital Numbers (DN) representing multispectral image data acquired by both the Operational Land Imager (OLI) and Thermal Infrared Sensor (TIRS). The products are in 16-bit unsigned integer format and need to be rescaled to the Top of Atmosphere (TOA) reflectance using radiometric rescaling coefficients provided in the product metadata file (MTL file). The following equation is used to convert DN values to TOA reflectance for OLI data as follows (USGS, 2013):

$$\rho\lambda' = M_\rho Q_{cal} + A_\rho \tag{2-1}$$

where $\rho\lambda'$ is TOA planetary reflectance (without correction for solar angle). M_ρ is Band-specific multiplicative rescaling factor from the metadata (REFLECTANCE_MULT_BAND_x, where x is the band number), A_ρ is band-specific additive rescaling factor from the metadata (REFLECTANCE_ADD_BAND_x, where x is the band number), and Q_{cal} is quantized and calibrated standard product pixel values (DN). Then, sun angle correction of TOA reflectance can be calculated by using the following equation (USGS 2013):

$$\rho\lambda = \frac{\rho\lambda'}{\cos(\theta sz)} = \frac{\rho\lambda'}{\sin(\theta se)} \tag{2-2}$$

Where $\rho\lambda$ is TOA planetary reflectance, θ_{SE} is local sun elevation angle. The scene center sun elevation angle in degrees is provided in the metadata (SUN_ELEVATION). θ_{SZ} is local solar zenith angle, $\theta_{SZ} = 90° - \theta_{SE}$.

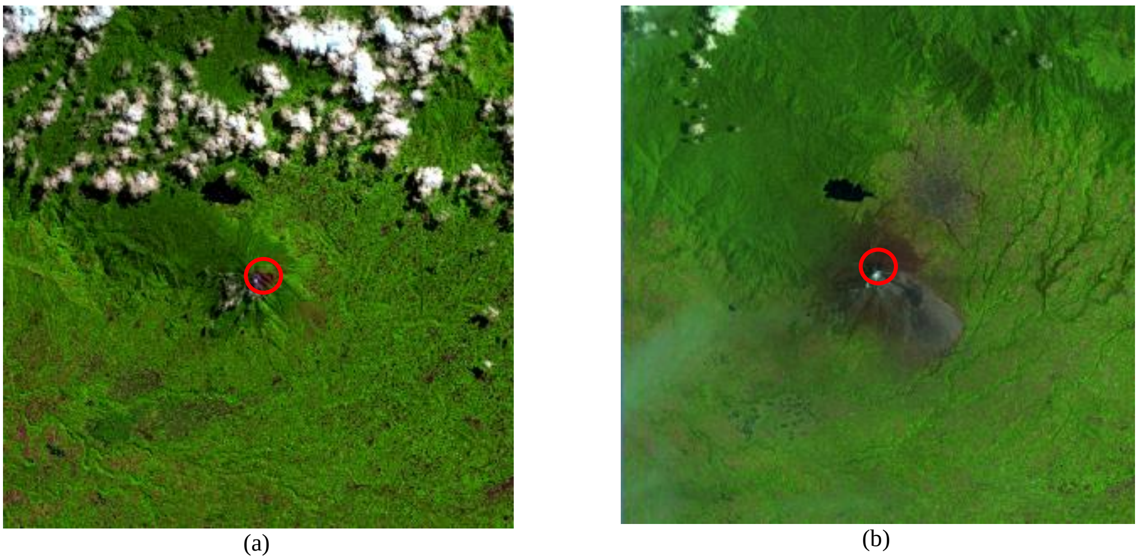

Figure 2-1: Landsat 8 used in this research. Showed in RGB composite 654 date 7th June 2013 (a: before eruption) and 22th March 2014 (b: after eruption). Red color show location of the crater of Mt. Sinabung

2.3 Delineation of Volcanic Region

Volcanic region is the area on the earth surface having forms and its characteristics which have been influenced by volcanism. Delineation the region of Volcanic was done visually from false color composite (FCC) RGB of Landsat 8, where Red=band 6, Green=5, and Blue=4. This image will present the natural color of earth surface. So, the land surface of stratovolcano Mt. Sinabung can be identified easier. For enhancing the images, the FCC have been sharpened with band 8 (15 meter resolution) using Brovey algorithm and transparency fusion with DEM SRTM by set up the sun angle of azimuth 45° and elevation 45°.

2.4 Topography Effect Correction

In mountainous areas there is a strong influence of the topography on the signal recorded by spaceborne optical sensors. In the same surface cover slopes oriented away from and towards the sun will appear darker and brighter, respectively, if compared to a horizontal geometry. This behavior causes problems for a subsequent scene classification and thematic evaluation (Richter et al., 2009). So, topographic correction methods were developed to reduce or eliminate the topographic influence.

C-correction method was implemented to reduce the topographic influence of Landsat 8 images which cover Mt. Sinabung region. C-correction is semi-empirical approach which is developed by Teillet et al. (1982). In operational of the project of INCAS (Indonesian National Carbon Accounting), this method were implemented for Landsat data processing (Trisakti et al., 2009). Below is the equation for calculating the corrected reflectance using the c-correction methods:

$$L_H = L_T \times \frac{\cos z + c}{\cos i + c} \qquad (2\text{-}3)$$

Where L_H is reflectance of a horizontal surface, L_T is reflectance of an inclined surface, z is solar zenith angle, i is local solar incident angle, c = b/m for L_T = m × cos i + b. m is gradient of regression line: L_T − cos i, and b is intercept of line: L_T − cos i. Cos i is the solar illumination angle between solar incident angle and local surface normal. Cos i varies from -1 (minimum) to +1 (maximum), which can be calculated as follows:

$$\cos i = \cos e \cos z + \sin e \sin z \cos (a - a') \qquad (2\text{-}4)$$

where i is local solar incident angle, e is slope angle, z is solar zenith angle, a is solar azimuth angle, and a' is aspect angle. Solar zenith angle and solar azimuth angle were provided in Landsat 8 metadata file (MTL), whereas slope angle and aspect angle can be derived from DEM SRTM.

2.5 Discrimination the Volcanic Eruption Products

Spectral signature of the products of volcanic eruption (lava, lava debris, lahar, and tephra) were derived from corrected reflectances of all Landsat 8 reflective bands. Both data date before and after eruption were calculated. Then, they will give the values which represent the conditions before and after eruption, also the changes from this period. These values is used as base values for detecting the affected area of Mt. Sinabung eruption. We implemented the thresholding methods based on reflectance change resulted from the statistics calculation to discriminate these regions.

3 RESULTS AND DISCUSSION

3.1 Volcanic Region's Delineation Result

Visual delineation from Landsat and DEM SRTM show the estimated boundaries of the volcanic region of Mt. Sinabung. Approximate area of of the regions is about 4,251 hectares. Figure 3-1 show estimated volcanic region of Mt. Sinabung. (a) and (b) were resulted processing of Landsat 8 FCC 654 pansharpened with band 8 using Brovey method date before (June 7, 2013) and after eruption (March 22, 2014), (c) and (d) are fusion with DEM SRTM for tranparency visualization.

3.2 The Results of Correction for Topographic Effect

The calculation of c-factor for c-correction of topographic effect for each band is shown on Table 3-1. Training sampel were taken just for forest cover on mountainous area. Figure 3-2 show a result of implementation of c-correction on Landsat 8. The corrected images show the corrected reflectance value in shaded topography. The uncorrected reflectance on the slope areas were shown darker.

Figure 3-3 show the reflectance values of affected area of Mt. Sinabung eruption in several landcovers. There are several types of changes, generally from vegetated area to barelands. Some types of the vegetated area are forest, shrub, and cultivated areas. The type of barelands are the vegetated areas previously which damaged and covered by eruption products such lava, lava debris, tephra, and ashfall

Table 3-1: The values of factor c for each band of Landsat 8

Band	b	m	c
1	0.083	0.001	63.923
2	0.063	0.002	39.438
3	0.047	0.004	11.850
4	0.029	0.003	10.556
5	0.190	0.040	4.708
6	0.078	0.017	4.565
7	0.029	0.006	4.742
8	0.039	0.003	12.516
9	0.001	0.000	30.000

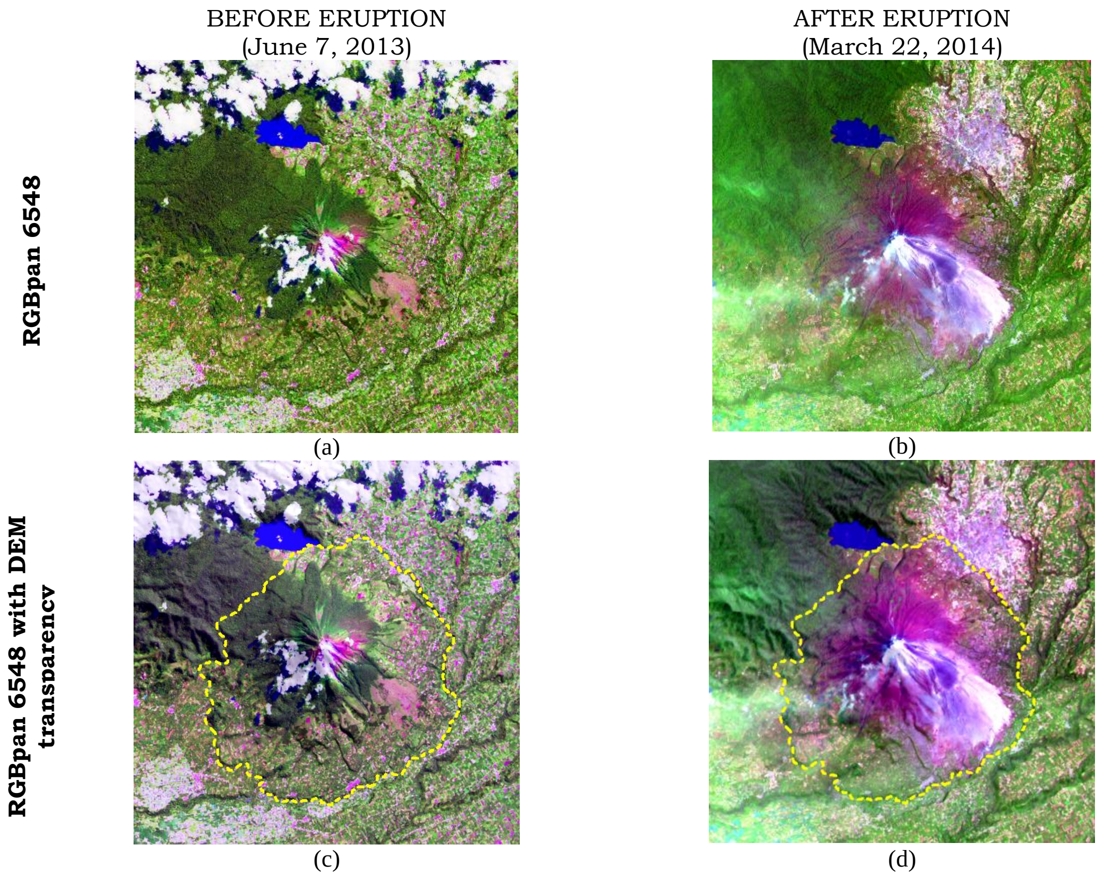

Figure 3-1: Delineation the region of Mt. Sinabung. Boundaries were shown by the dotted yellow line

So, several kinds of cover changes are changes from forest to lava, forest to lava debris, shrub to tephra, cultivated area to ashfall. Another important thing for detection the volcanic eruption products is that changing from barren to bareland which covered by volcanic eruption products. So, such analysis also be done from barren to barelands.

Band 5 (0.845 – 0.885 µm) and Band 6 (1.560 – 1.660 µm) is the two most sensitive bands for the detection among all cover types among forests, shrubs, cultivated areas, and also barelands. The changing from forest to lava (forest totally replaced by lava) indicated the increasing reflectance values of all visible bands (band 1, 2 , 3, and 4) and $SWIR_L$ (band 7). Otherwise, there were decreasing of reflectance values of band 5 (NIR) and band 6 ($SWIR_S$). This pattern was the same as the changing from shrub to lava debris (shrub covered totally by lava debris).

The changes from forest to tephra (forest totally covered by abundant of tephras) indicated the increasing reflectance values of all bands (band 1, 2, 3, 4, 6 and 7) except band 5, the reflectance values of band 5 will decrease. This pattern was the same as the changing from shrub to tephra (shrub totally covered by abundant of tephras) and also the changes from cultivated areas to ashfall (cultivated areas covered by ashfalls). There is the unique pattern of the changing from barren to tephra (bareland consists of older volcanic material, changes to bareland, the areas covered by new volcanic materials). The changing were indicated by increasing values of all visible bands (band 1, 2, 3, and 4).

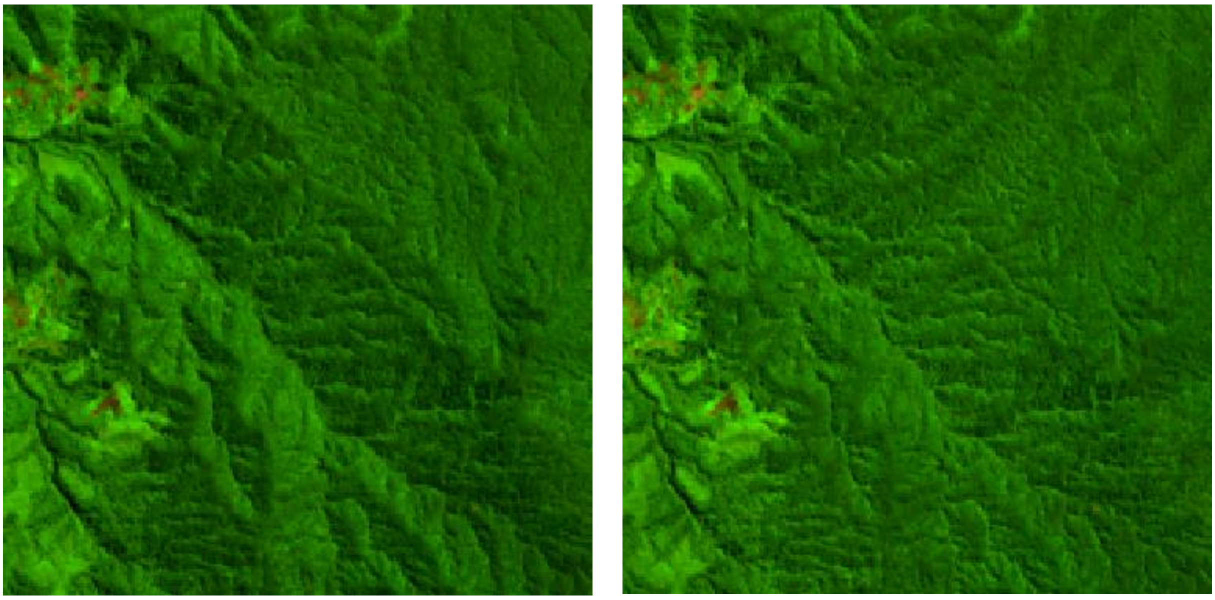

(a) Original images (b) Corrected images

Figure 3-2: Result of the effect topography correction on Landsat 8 using c-correction method. The images were displayed on FCC RGB 654

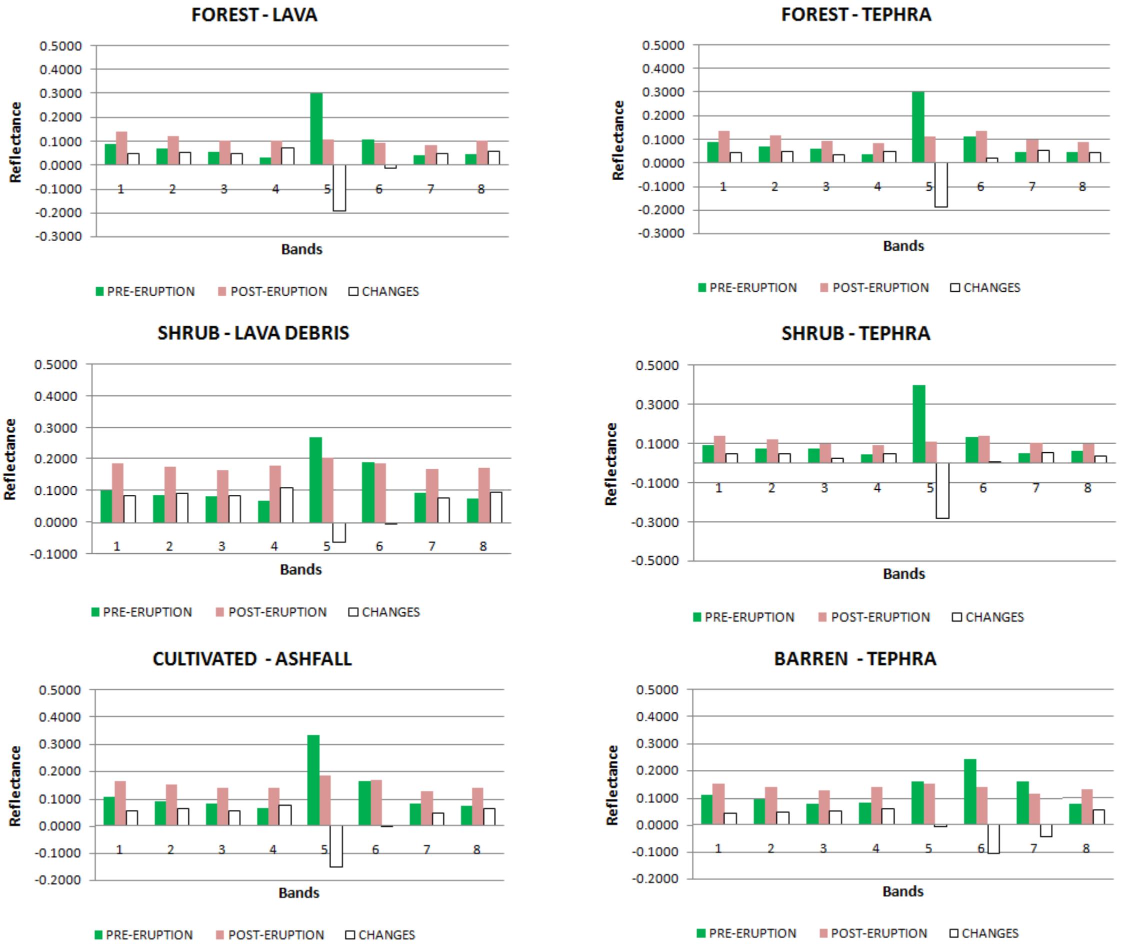

Figure 3-3: Reflectance values of affected area of Mt. Sinabung eruption each surface cover (pre-eruption, after eruption and its changes)

Table 3-2: The changes of reflectance values from forest to lava (forest totally replaced by lava)

	Band	1	2	3	4	5	6	7	8
Pre- Eruption	Mean	0.0896	0.0686	0.0559	0.0323	0.3006	0.1089	0.0393	0.0455
	Dev.std	0.0006	0.0006	0.0013	0.0010	0.0164	0.0052	0.0022	0.0020
Post- Eruption	Mean	0.1385	0.1226	0.1030	0.1033	0.1084	0.0937	0.0851	0.1034
	Dev.std	0.0028	0.0032	0.0042	0.0052	0.0063	0.0060	0.0052	0.0048
Changes	Mean	0.0488	0.0540	0.0471	0.0709	-0.1922	-0.0153	0.0459	0.0579
	Dev.std	0.0029	0.0032	0.0040	0.0051	0.0164	0.0063	0.0047	0.0049

Table 3-3: The changes of reflectance values from forest to tephra (forest covered totally by abundant of tephras)

	Band	1	2	3	4	5	6	7	8
Pre- Eruption	Mean	0.0897	0.0693	0.0583	0.0349	0.3012	0.1131	0.0442	0.0479
	Dev.std	0.0008	0.0009	0.0021	0.0018	0.0219	0.0087	0.0051	0.0027
Post- Eruption	Mean	0.1332	0.1150	0.0904	0.0847	0.1128	0.1332	0.0967	0.0889
	Dev.std	0.0020	0.0022	0.0024	0.0028	0.0083	0.0068	0.0048	0.0038
Changes	Mean	0.0435	0.0457	0.0322	0.0498	-0.1885	0.0201	0.0525	0.0410
	Dev.std	0.0021	0.0022	0.0031	0.0029	0.0232	0.0097	0.0056	0.0041

Table 3-4: The changes of reflectance values from shrub to lava debris (shrub covered totally by lava debris)

	Band	1	2	3	4	5	6	7	8
Pre- Eruption	Mean	0.1020	0.0846	0.0814	0.0687	0.2674	0.1911	0.0924	0.0745
	Dev.std	0.0009	0.0010	0.0016	0.0022	0.0075	0.0050	0.0031	0.0026
Post-Eruption	Mean	0.1852	0.1755	0.1655	0.1799	0.2051	0.1857	0.1703	0.1707
	Dev.std	0.0024	0.0027	0.0035	0.0046	0.0050	0.0053	0.0053	0.0049
Changes	Mean	0.0832	0.0909	0.0842	0.1112	-0.0623	-0.0054	0.0779	0.0963
	Dev.std	0.0024	0.0028	0.0041	0.0052	0.0093	0.0080	0.0063	0.0057

Table 3-5: The changes of reflectance values from shrub to tephra (shrub totally covered by abundants of tephra)

	Band	1	2	3	4	5	6	7	8
Pre- Eruption	Mean	0.0911	0.0723	0.0727	0.0447	0.3955	0.1335	0.0513	0.0601
	Dev.std	0.0020	0.0023	0.0055	0.0047	0.0129	0.0171	0.0096	0.0058
Post-Eruption	Mean	0.1358	0.1189	0.0969	0.0928	0.1115	0.1411	0.1045	0.0958
	Dev.std	0.0027	0.0032	0.0037	0.0050	0.0057	0.0100	0.0070	0.0047
Changes	Mean	0.0448	0.0466	0.0242	0.0481	-0.2840	0.0076	0.0532	0.0356
	Dev.std	0.0024	0.0026	0.0044	0.0042	0.0119	0.0212	0.0115	0.0049

Table 3-6: The changes of reflectance value from cultivated areas to ashfall (cultivated areas covered by ashfall)

	Band	1	2	3	4	5	6	7	8
Pre- Eruption	Mean	0.1078	0.0898	0.0836	0.0645	0.3352	0.1658	0.0825	0.0744
	Dev.std	0.0094	0.0108	0.0110	0.0167	0.0738	0.0267	0.0219	0.0150
Post-Eruption	Mean	0.1638	0.1532	0.1397	0.1408	0.1847	0.1676	0.1292	0.1393
	Dev.std	0.0058	0.0073	0.0090	0.0115	0.0155	0.0137	0.0119	0.0109
Changes	Mean	0.0560	0.0634	0.0561	0.0763	-0.1505	0.0018	0.0466	0.0649
	Dev.std	0.0087	0.0100	0.0102	0.0148	0.0721	0.0268	0.0213	0.0142

Table 3-7: The changes of reflectance values from barren to tephra

	Band	1	2	3	4	5	6	7	8
Pre- Eruption	Mean	0.1101	0.0938	0.0774	0.0797	0.1588	0.2427	0.1596	0.0769
	Dev.std	0.0043	0.0055	0.0067	0.0090	0.0263	0.0495	0.0374	0.0092
Post-Eruption	Mean	0.1534	0.1412	0.1292	0.1375	0.1524	0.1382	0.1140	0.1315
	Dev.std	0.0062	0.0072	0.0097	0.0139	0.0153	0.0168	0.0171	0.0141
Changes	Mean	0.0433	0.0474	0.0518	0.0577	-0.0065	-0.1045	-0.0455	0.0546
	Dev.std	0.0084	0.0099	0.0134	0.0199	0.0349	0.0615	0.0518	0.0194

Table 3-8: The changes of reflectance values from all surface covers to volcanic deposits

	Band	1	2	3	4	5	6	7	8
Pre- Eruption	Mean	0.0994	0.0804	0.0725	0.0527	0.3118	0.1487	0.0692	0.0632
	Dev.std	0.0106	0.0121	0.0142	0.0192	0.0641	0.0396	0.0309	0.0165
Post-Eruption	Mean	0.1531	0.1395	0.1222	0.1227	0.1537	0.1498	0.1182	0.1222
	Dev.std	0.0182	0.0217	0.0272	0.0327	0.0401	0.0283	0.0263	0.0290
Changes	Mean	0.0537	0.0590	0.0497	0.0700	-0.1581	0.0011	0.0489	0.0590
	Dev.std	0.0133	0.0153	0.0181	0.0215	0.0738	0.0316	0.0265	0.0199

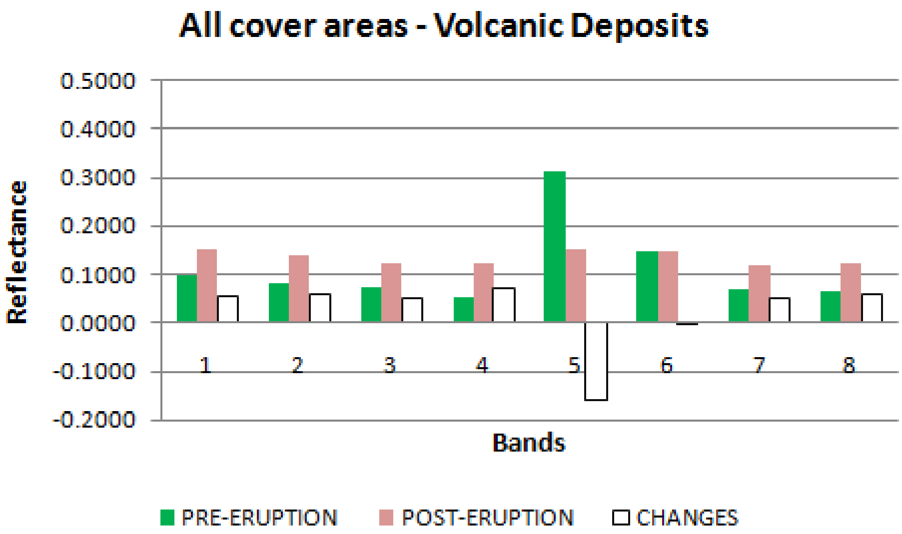

Figure 3-4: The changes of reflectance values of all landcovers (turn into volcanic deposits)

Based on pattern of the reflectance changes, then NDVI value were also calculated. From the spectral response, it can be seen that generally there were high values on NIR (band 5) and low values on Red (band 4). Also, there were highest decreasing values on band 5 and there were highest increasing on band 4. So, combination of the two bands, they can be used to detecting the change of surface cover due to volcanic eruption. The NDVI is an index that be derived from both bands. The NDVI values derived from Landsat 8 were calculated by using the following aquation:

$$NDVI = \frac{\rho 5 - \rho 4}{\rho 5 + \rho 4} \quad (3\text{-}1)$$

Where ρ4 and ρ5 are reflectance values of band 4 and 5 respectively. Then, normalized distance (D values) were calculated to measure and to test the discrimination ability of the index (Kaufman & Remer, 1994). The D-values > 1 will represent good separability of the index to discriminate the volcanic deposits and non volcanic deposits. Below is the equation for calculating D-values.

$$D = \left| \frac{\mu 2 - \mu 1}{\sigma 2 + \sigma 1} \right| \quad (3\text{-}2)$$

Where D is Normalized Distance, μ1 and μ2 are mean values of samples before and after eruption respectively, σ1 and σ2 are standard deviation of samples before and after eruption respectively. The results calculation of the D-value for all bands and NDVI as shown below (Table 3-9). The variables of ρ1, ρ2, ρ3, ρ4, ρ5, ρ8, and NDVI showed the D-value>1, therefore they have good separabilty to discriminate the volcanic deposits and non volcanic deposits. Then, implementation among variables were done using the threshold based on mean (μ) and deviation standard (σ) values (Table 3-10).

Then ρ1, ρ2, ρ3, ρ4, ρ5, ρ8, and NDVI were tested using the criterias based on the mean and deviation standard for extracting the affected areas of volcanic eruption from lava, lava debris, tephra and ashfall (Figure 3-5). The results show that NIR (band 5) individually and NDVI can be used to detect and separate the volcanic eruption products. But, NDVI seem to give the better result rather than band 5. Another band may be used to detected them, but it was difficult for separating from non volcanic eruption products due to high commision error.

Table 3-9: the *D*-values for spectral bands and NDVI of Landsat 8

Variables	D-value
ρ1	1.868
ρ2	1.745
ρ3	1.201
ρ4	1.349
ρ5	1.516
ρ 6	0.017
ρ7	0.856
ρ8	1.296
NDVI	3.216

Table 3-10: The mean and deviation standard for ρ1, ρ2, ρ3, ρ4, ρ5, ρ8, and NDVI

	Post Eruption		Change	
	Mean	SD	Mean	SD
ρ1	0.1531	0.0182	0.0537	0.0133
ρ2	0.1395	0.0217	0.0590	0.0153
ρ3	0.1222	0.0272	0.0497	0.0181
ρ4	0.1227	0.0327	0.0700	0.0215
ρ5	0.1537	0.0401	-0.1581	0.0738
ρ8	0.1222	0.0290	0.0590	0.0199
NDVI	0.1121	0.0524	-0.5987	0.1301

For comparative data, the estimated distribution of deposits eruption (lava and pyroclastic) analyzed data from TerraSAR-X dated January 18, 2014 (Source: Disaster Charter Activation), shown in Figure 3-6. Although there is little difference in the date, assuming that no major eruptive activity in the period from 18 January to March 22, 2014, this data can be used as a comparison. In comparison, it is known that the results of the analysis with parameters NDVI, give the best results are similar to the results of the data analysis using TerraSAR-X. Furthermore, based on Geologic Map of Sinabung Volcano (Prambada et al., 2011), the affected areas of Mount Sinabung detected from NDVI parameter really is an area exposed to direct attack from the products eruptions such as lava and pyroclastic. The geological is dominantly composed of the youngest lava rock units deposited toward the Southeast with a thickness of 4 meters outcrop. This units form a rough morphology which covered a pyroclastic flow. The pyroclastic flow was deposited in the south eastern Mt. Sinabung.

4 CONCLUSION

The use of Landsat 8 OLI for detecting the affected areas of Mt. Sinabung eruption has showed that band 5 is the most sensitive band for the detection of all cover types among forests, shrubs, cultivated areas, and also for barelands on the volcanic region. The changing of reflectance values from all type cover areas (forest, shrub, cultivated, and barren) to volcanic deposits (lava, lava debris, tephra, and ashfall) were indicated by increasing values of all bands except band 5.

Band 5 showed the highest values of decreasing and band 4 showed the highest values of increasing. Compared with another uses of single band, the combination of both bands (NDVI) give the best result for detecting the affected areas of volcanic eruption.

As comparative data, based on the estimated distribution of deposits eruption (lava and pyroclastic) analyzed data from TerraSAR-X and Geologic Map of Sinabung Volcano, can be seen that the affected areas of Mount Sinabung detected from NDVI parameter, really is an area exposed to direct attack from the products eruptions such as lava flow and pyroclastic.

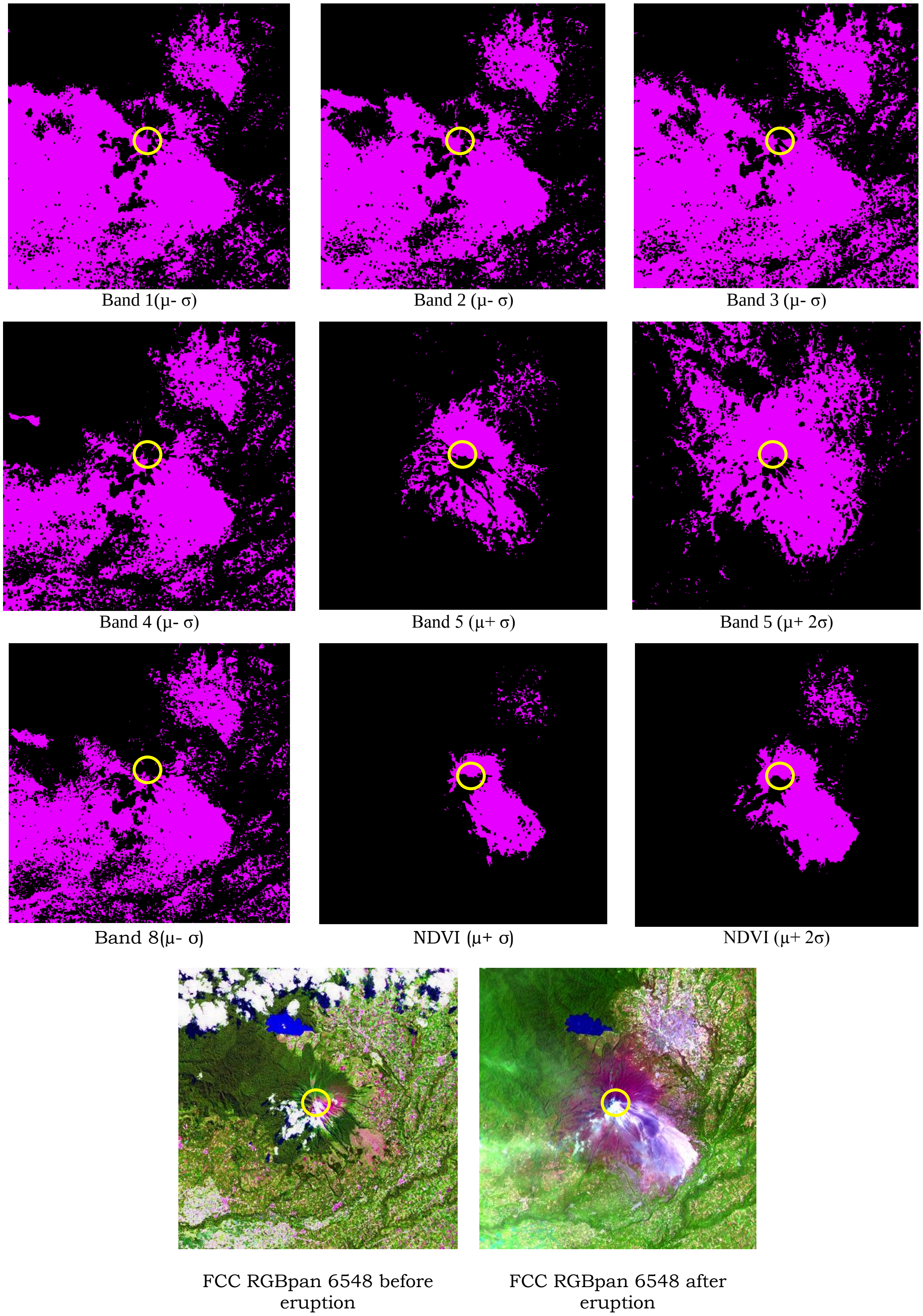

Figure 3-5: Implementation the variable of ρ1, ρ2, ρ3, ρ4, ρ5, ρ8, and NDVI for extracting the affected areas of volcanic eruption (from lava, lava debris, tephra and ashfall) using the criterias based on the mean and standard deviation. Yellow color show location of the crater of Mt. Sinabung.

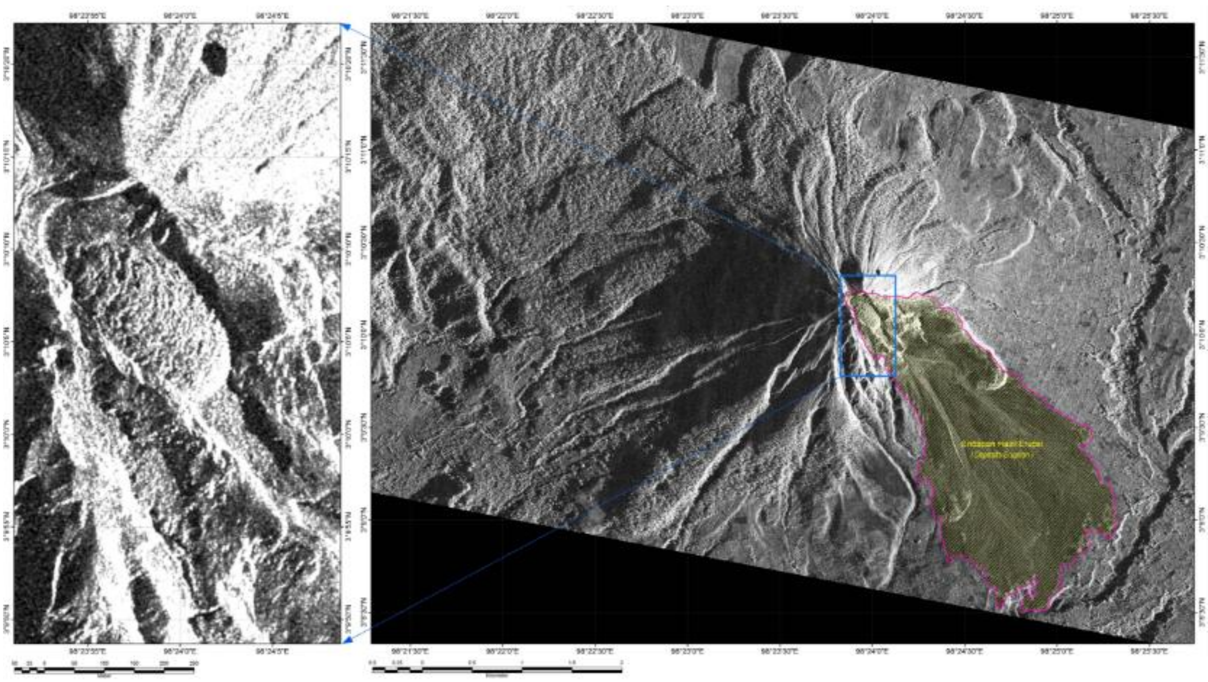

Figure 3-6: The estimated distribution of deposits eruption (lava and pyroclastic) analyzed data from TerraSAR-X dated January 18, 2014 (Source: Disaster Charter Activation. URL: https: //www.disasterscharter.org/web/guest/-/volcano-in-indones-2)

ACKNOWLEDGEMENT

This paper was part of a research program with the title "Pengembangan Model Pemanfaatan Penginderaan Jauh Untuk Pemetaan Cepat Daerah Terkena Bencana Erupsi Gunungapi" (Model Development of the Application of Remote Sensing for Rapid Mapping of the Affected Area of the Volcanic Eruption) in Remote Sensing Application Center of LAPAN. The paper had previously been presented at the 12th Biennial Conference of Pan Ocean Remote Sensing Conference PORSEC 2014 under the title "Detecting the Affected Areas of Mount Sinabung Eruption Using Landsat 8 Based on Reflectance Change" and also was published in its proceedings. With some improvement then this paper finally published in this journal.

Thanks Dr. Bambang Trisakti and Dr. Baba Barus who have given advices for improvement in this paper. Thank Director of Remote Sensing Technology and Data Center of LAPAN and staffs who have provided the Landsat 8.

REFERENCES

Benoît SB, Christelle W, d'Oreye N., (2010), A new map of the lava flow field of Nyamulagira (D.R. Congo) from satellite imagery. Journal of African Earth Science 58:778-786.

Davila N, Capra L, Gavilanes-Ruiz JC, Varley N, Norini G, Vazquez AG., (2007), Recent lahars at Volcán de Colima (Mexico): Drainage variation and spectral classification. Journal of Volcanology and Geothermal Research 165:127-141.

Flynn LP, Harris AJL, Wright R., (2001), Improved identification of volcanic features using Landsat 7 ETM+. Remote Sensing of Environment 78: 180-193.

Harris AJL, Flynn LP, Keszthelyi L, Mouginis-Mark PJ, Rowland SK, Resing JA., (1998), Calculation of lava effusion rates from Landsat TM data. Bull Volcanol 60: 52-71.

http://www.vsi.esdm.go.id/index.php/gunungapi/aktivitas-gunungapi/622-evaluasi-tingkat-aktivitas-siaga-level-iii-g-sinabung-hingga-tanggal-11-september-2014. Accessed on Oktober 18, 2014.

https://www.disasterscharter.org/web/guest/-/volcano-in-indones-2) ; Accessed on April 1, 2015.

Irons JR, Dwyer JL, Barsi JA., (2012), The next Landsat satellite: The Landsat Data Continuity Mission. Remote Sensing of Environment 122:11-21.

Kaufman YJ, Remer LA., (1994), Detection of forest fire using Mid-IR reflectance: and application fro aerosols study. IEEE Transactions on Geoscience and Remote Sensing 32: 672-683.

Kusumadinata K., (1979), Data dasar gunung api indonesia. Direktorat Vulkanologi, Bandung. (In Indonesian).

Lombardo V, Buongiorno MF, Pieri D, Merucci L., (2004), Differences in Landsat TM derived lava flow thermal structures during summit and flank eruption at Mount Etna. Journal of Volcanology and Geothermal Research 134: 15-34.

Novak ID, Soulakellis N., (2000), Identifying geomorphic features using LANDSAT-5 TM data processing techniques on Lesvos, Greece. Geomorphology 34: 101-109.

Prambada O, Zaenuddin A, Iryanto, Santosa I, Nakada N., Yoshimoto M., (2009), Geological Map of Sinabung Volcano, North Sumatera Province. Center for Volcanology and Geological Hazard Mitigation, Geological Agency, Ministry of Energy and Mineral Resources.

Ritcher R, Kellenberger T, Kaufmann H., (2009), Comparison of Topographic Correction Methods. Remote Sensing 1: 184-196.

Sutawidjaja IS, Prambada O, Siregar DA., (2013), The August phreatic eruption of Mount Sinabung, North Sumatra. Indonesian Journal of Geology 8:55-61.

Teillet P, Guindon B, Goodenough D., (1982), On the slope-aspect correction of Multispectral Scanner Data. Canadian Journal of Remote Sensing 8: 84-106.

Trisakti B., Kartasasmita M, Kustiyo, Kartika T., (2009), Kajian koreksi terrain pada citra Landsat Thematic Mapper (TM). Jurnal Penginderaan Jauh dan Pengolahan Data Citra Digital 6: 1-10 (In Indonesian).

USGS, (2013), http://landsat.usgs.gov; Accessed on April 16, 2013.

Wright R, Flynn LP, Harris AJL., (2001), Evolution of lava flow-fields at Mount Etna, 27-28 October 1999, observed by Landsat 7 ETM+. Bull Volcanol 63: 1-7.